European Radiology (2019) 29:4068–4076
https://doi.org/10.1007/s00330-018-5830-3

NEURO

Radiomics and machine learning may accurately predict the grade and histological subtype in meningiomas using conventional and diffusion tensor imaging

Yae Won Park[1,2] · Jongmin Oh[3] · Seng Chan You[4] · Kyunghwa Han[2] · Sung Soo Ahn[2] · Yoon Seong Choi[2] · Jong Hee Chang[5] · Se Hoon Kim[6] · Seung-Koo Lee[2]

Received: 17 August 2018 / Revised: 19 September 2018 / Accepted: 12 October 2018 / Published online: 15 November 2018

Abstract

Objectives Preoperative, noninvasive prediction of the meningioma grade is important because it influences the treatment strategy. The purpose of this study was to evaluate the role of radiomics features of postcontrast T1-weighted images (T1C), apparent diffusion coefficient (ADC), and fractional anisotropy (FA) maps, based on the entire tumor volume, in the differentiation of grades and histological subtypes of meningiomas.

Methods One hundred thirty-six patients with pathologically diagnosed meningiomas (108 low-grade [benign], 28 high-grade [atypical and anaplastic]), who underwent T1C and diffusion tensor imaging, were included in the discovery set. The T1C image, ADC, and FA maps were analyzed to derive volume-based data of the entire tumor. Radiomics features were correlated with meningioma grades and histological subtypes. Various machine learning classifiers were trained to build classification models to predict meningioma grades. We tested the model in a validation set (58 patients; 46 low-grade; 12 high-grade).

Results The machine learning classifiers showed variable performances depending on the machine learning algorithms. The best classification system for the prediction of meningioma grades had an area under the curve of 0.86 (95% confidence interval [CI], 0.74–0.98) in the validation set. The accuracy, sensitivity, and specificity of the best classifier were 89.7, 75.0, and 93.5% in the validation set, respectively. Various texture parameters differed significantly between fibroblastic and non-fibroblastic subtypes.

Conclusions Radiomics feature-based machine learning classifiers of T1C images, ADC, and FA maps are useful for differentiating meningioma grades.

Key Points

- *Preoperative, noninvasive differentiation of the meningioma grade is important because it influences the treatment strategy.*
- *Radiomics feature-based machine learning classifiers of T1C images, ADC, and FA maps are useful for differentiating meningioma grades.*
- *In benign meningiomas, there were significant differences in the various texture parameters between fibroblastic and non-fibroblastic meningioma subtypes.*

Keywords Diffusion tensor imaging · Magnetic resonance imaging · Meningioma · Radiomics

Electronic supplementary material The online version of this article (https://doi.org/10.1007/s00330-018-5830-3) contains supplementary material, which is available to authorized users.

✉ Sung Soo Ahn
sungsoo@yuhs.ac

[1] Department of Radiology, Ewha Womans University College of Medicine, Seoul, South Korea

[2] Department of Radiology and Research Institute of Radiological Science, Yonsei University College of Medicine, 50-1 Yonsei-ro, Seodaemun-gu, Seoul 120-752, South Korea

[3] Department of Convergence Medicine, Ewha Womans University College of Medicine, Seoul, South Korea

[4] Department of Biomedical Informatics, Ajou University School of Medicine, Suwon, South Korea

[5] Department of Neurosurgery, Yonsei University College of Medicine, Seoul, South Korea

[6] Department of Pathology, Yonsei University College of Medicine, Seoul, South Korea

Abbreviations

ADC	Apparent diffusion coefficient
AUC	Area under the curve
DTI	Diffusion tensor imaging
FA	Fractional anisotropy
T1C	Postcontrast T1-weighted image

Introduction

Meningiomas are the most common primary intracranial neoplasms in adults, comprising 36.7% of all intracranial tumors [1]. According to the World Health Organization (WHO) classification system, 78% are benign (grade I), 20.4% are atypical (grade II), and 1.6% are anaplastic (grade III) [2]. Atypical or anaplastic tumors have an aggressive biological behavior, a tendency to recur [3], and a poor prognosis, with 5-year survival rates of 67.5 and 60.0% for patients with atypical and anaplastic meningiomas, respectively.

The initial extent of tumor resection and histological grade are key determinants of recurrence [4]. Thus, preoperative prediction of the meningioma grade is important because it influences treatment planning, including the surgical resection strategy. Further, according to the recent guideline published by the European Association of Neuro-Oncology [5], incidentally discovered and radiologically presumed meningiomas may be managed by observation only; thus, histological verification is not mandatory in these cases. Considering the numbers of tumors that are managed without histopathologic diagnosis, it is important to noninvasively differentiate between low-grade and high-grade meningiomas.

According to the 2016 WHO classification, benign meningiomas differ from atypical meningiomas in their numbers of mitoses, cellularity, nucleus-to-cytoplasm ratio, and brain invasion, as well as in their histologic patterns. The different histological grade may reflect alterations in tumor cell proliferation and microvessel density, which may be related to the characteristic imaging features. Diffusion tensor imaging (DTI) provides information regarding the motion of water protons at the cellular level [6], and the directional restriction of water diffusivity can be measured as the fractional anisotropy (FA); however, previous studies have shown controversial results regarding the prediction of the meningioma grade using diffusion-weighted imaging or DTI values [7–13].

Additionally, previous studies have investigated imaging features to predict the meningioma grade within conventional imaging approaches, including tumor heterogeneity on postcontrast T1-weighted (T1C) images, as well as irregular tumor margin and peritumoral brain edema [14–16]; however, these qualitative imaging features are highly subjective. In contrast, radiomics provides a comprehensive quantification of tumor phenotypes noninvasively by extracting a large number of high-throughput imaging features, such as shape and texture, potentially reflecting biologic properties, especially tumor heterogeneity. Recent studies using radiomics have shown promising results in differentiating molecular subtypes and predicting survival in gliomas [17–19].

In benign meningiomas, tumor consistency is important in determining the surgical outcome. Fibroblastic subtypes have been reported to exhibit a firmer tumor consistency, which thus requires painstaking dissection, especially for tumors located at the skull base [20]. Thus, preoperative information regarding the histological subtypes of meningiomas is also important.

The purpose of this study was to evaluate the role of radiomics features including texture and morphology of T1C images and DTI parameters, based on the entire tumor volume, in preoperatively determining the grades and histological subtypes of meningiomas.

Methods

Patient population

The institutional review board waived the requirement to obtain informed patient consent for this retrospective study. We retrospectively reviewed meningioma cases in which pathological confirmation, preoperative MRI with T1C image, and whole-brain DTI with a b value of 600 s/mm^2 were performed. Exclusion criteria were the following: (1) patients with a previous history of operation, (2) patients with a history of tumor embolization or gamma knife surgery before the MRI exam, (3) patients with incomplete MRI sequences or suboptimal image quality, and (4) error in image processing. The study population was chronologically divided into two sets. First, 136 consecutive patients (108 low-grade [benign], 28 high-grade [atypical and anaplastic]), diagnosed as having meningiomas between June 2010 and October 2016, were included in the discovery set (108 women and 28 men; mean age, 56.00 ± 12.93 years), and 58 consecutive patients (46 low-grade, 12 high-grade), diagnosed as having meningiomas between November 2016 and March 2018, were included in the validation set (44 women and 14 men; mean age, 59.24 ± 13.17 years). The mean interval between the MRI examination and operation was less than 1 day for all patients. The flow chart of the study population is shown in Fig. 1.

Pathological diagnosis

Pathological diagnosis was performed by a neuropathologist (S.H.K., 16 years of experience), according to the 2016 WHO criteria [21]. Criteria for atypical meningioma (WHO grade II) comprised 4–19 mitoses per 10 high-power fields, the presence of brain invasion, or the presence of at least three of these features ("sheet-like" growth, hypercellularity, spontaneous

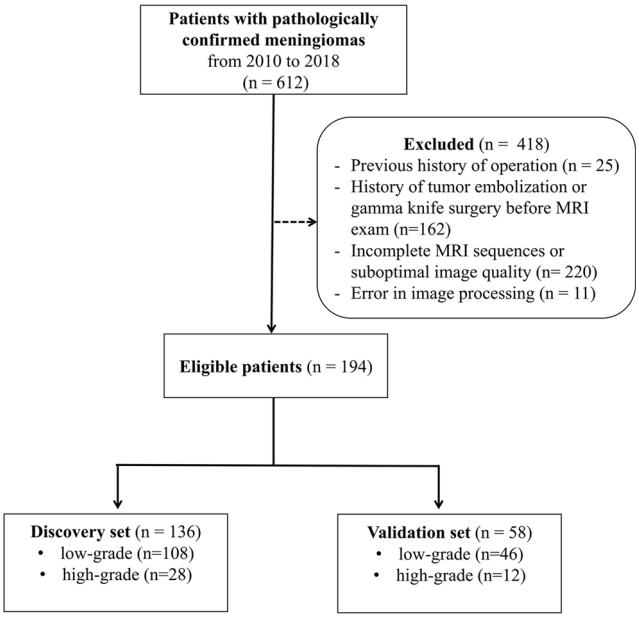

Fig. 1 The flowchart for the discovery and validation set

necrosis, large and prominent nucleoli, and small cells); criteria for anaplastic meningioma (WHO grade III) comprised frank anaplasia (histology resembling carcinoma, sarcoma, or melanoma) or elevated mitoses (> 20 mitoses per 10 high-power fields) [21]. Additionally, the Ki-67 labeling index was evaluated in 187 patients. In 152 of 194 patients, the mitotic count was evaluated using the mitotic marker phosphohistone-H3.

MRI protocol

Preoperative MRI was performed using a 3.0-T MRI scanner (Achieva, Philips Medical Systems) with an eight-channel sensitivity-encoding head coil. The preoperative MRI protocol included T1-weighted (T1) (TR/TE 2000/10 ms; field of view, 230 mm; section thickness, 5 mm; and matrix, 320 × 198) and T1C (TR/TE, 2000/10 ms; field of view, 250 mm; section thickness, 2 mm; and matrix, 256 × 256) images, as well as whole-brain DTI (with b values of 600 and 0 s/mm^2, 32 directions, and the following parameters: TR/TE, 8400–8500/70–80 ms; field of view, 220 mm; section thickness, 2 mm; matrix, 112 × 112; acceleration factor, 2.5; and acquisition time, 5 min and 20 s). T1C images were acquired after administration of 0.1 mL/kg of gadolinium-based contrast material (Gadovist; Bayer).

Image preprocessing and postprocessing: volume acquisition

Data processing was performed offline. Preprocessing of the T1C images was performed to standardize the data analysis across patients. Before analysis, unwanted low-frequency intensity nonuniformity was removed by applying the N4 bias correction algorithm [22]. T1C image intensities were normalized using WhiteStripe [23] packages, implemented in R version 3.4.0 (R Foundation for Statistical Computing). T1C image and DTI data were processed with a multi-platform, free, and open-source software package for visualization and medical image computing (3D slicer, version 4.6.2-1; available at: http://slicer.org/). T1C images were coregistered to ADC and FA maps by affine transformation with normalized mutual information as a cost function [24–26]; ROIs were drawn on every tumor section on T1C images, using a semiautomatic method with an interactive level-set volume of interest using threshold-based and edge-based algorithms. Gross cystic, hemorrhagic, or necrotic areas were avoided by using conventional T1 and T1C images. The ROIs were transferred to ADC and FA maps. The ROIs were drawn by a single neuroradiologist and confirmed by another neuroradiologist (Y.W.P. and S. S.A., with 7 and 12 years of experience, respectively), both of whom were blinded to the corresponding clinical information and histopathologic results.

In total, 90 texture features (T1C, ADC, FA maps × 30 features, belonging to three categories) and eight morphology features were calculated (Supplementary Table 1). The three categories of texture features included histogram-based, co-occurrence matrix-based, and run-length matrix-based parameters. Detailed information regarding these features can be found in previous literature [27, 28]. A schematic for the data processing is shown in Fig. 2.

Statistical analysis

The correlations between radiomics features and the meningioma grade were assessed using Student's t test or the Mann-Whitney test according to the normality tests.

Machine learning classifiers from various combinations of feature subset selection, machine learning methods, and subsampling were trained to predict the meningioma grade. For feature subset selection, either no subset selection or recursive feature elimination (RFE) was performed. These feature selection methods were combined with support vector machine (SVM) and random forest (RF) machine learning methods. In addition, to overcome disparity in the frequencies of the meningioma grade, each machine learning model was trained (1) without subsampling, (2) with random over-sampling examples (ROSE), and (3) with the synthetic minority over-sampling technique (SMOTE) [29, 30]. Thus, a total of 12 combinations of feature subset selection, machine learning algorithm, and subsampling were trained and validated to classify the tumor grade.

Machine learning classifiers were trained on the discovery set (n = 136) and validated on the validation set (n = 58). For each machine learning combination, we trained the model on the discovery set using leave-one-out cross validation. The classifier yielded predicted probabilities for the meningioma grade. The area under the curve (AUC), accuracy, sensitivity,

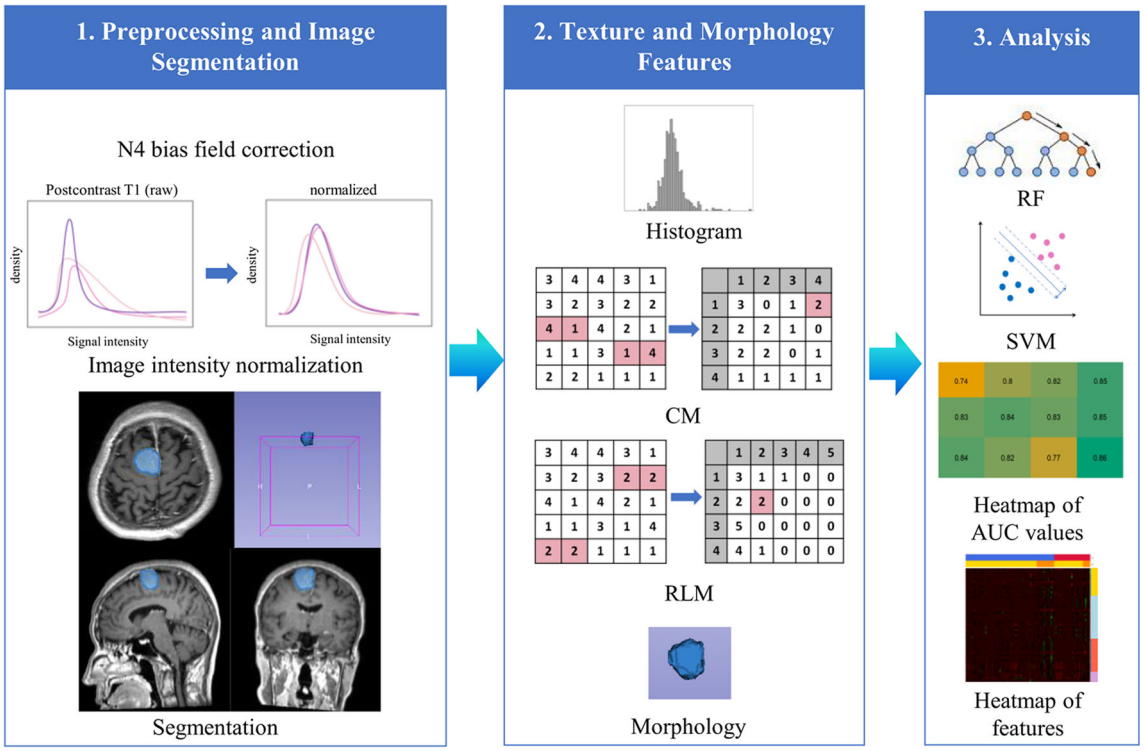

Fig. 2 The workflow for imaging data processing and analysis. CM, co-occurrence matrix; RLM, run-length matrix; RF, random forest; SVM, support vector machine; AUC, area under the curve

and specificity were calculated. A hypothesis test was performed (with the binom.test function) to evaluate whether the accuracy rate is higher than the no-information rate (the majority percentage for the meningioma grade, i.e., prediction by chance). Also, the precision-recall plots were calculated.

The correlation between radiomics features with the mitosis count and the Ki-67 labeling index was evaluated by Pearson correlation coefficient analysis.

Benign meningiomas were subdivided into fibroblastic meningiomas and other subtypes. Correlations between texture and morphology parameters and subgroups were assessed using Student's *t* test or the Mann-Whitney test, according to the results of normality testing.

Statistical analysis was performed (by J.M.O., a biostatistician with 5 years of experience in computational biology) using statistical software R (version 3.3.1; R Foundation for Statistical Computing). The RFE feature selection and classification algorithms were performed using the caret R package [31]. ROSE and SMOTE subsampling were performed using the ROSE and DMwR R packages [32, 33]. The e1071 and pROC packages were used. Statistical significance was set at $p < 0.05$.

Results

Characteristics of the 194 patients in the discovery ($n = 136$) and validation ($n = 58$) sets are summarized in Table 1. In the discovery set, 108 patients were pathologically diagnosed with low-grade meningioma and 28 were diagnosed with high-grade meningioma (25 atypical, three anaplastic). In the validation set, 46 were pathologically diagnosed with low-grade meningioma and 12 were diagnosed with high-grade meningioma (11 atypical, one anaplastic).

Radiomics feature analyses for determining meningioma grades

Various radiomics features were significantly different according to the meningioma grade (Supplementary Table 2). According to texture features, high-grade meningiomas showed higher histogram entropy, dissimilarity, coarseness, and less homogeneity along the run lengths of T1C, ADC, and FA values. For the morphology features with discriminative ability, high-grade meningiomas present as larger volumes with larger maximum 3D diameter and are more compact (higher "compactness 1," defined as the ratio of volume to the [surface area]$^{\wedge 1.5}$) [34] than low-grade meningiomas. Supplementary Fig. 1 shows representative cases that manifest the texture and morphology differences between different meningioma grades.

The performances of machine learning models in differentiating the meningioma grade in the validation set are demonstrated in Table 2. The AUC values from various machine learning classifiers to predict the grade are shown in Fig. 3.

Table 1 Patient characteristics in the discovery and validation sets

	Discovery set ($n = 136$)		Validation set ($n = 58$)		p value *
	Low-grade ($n = 108$)	High-grade ($n = 28$)	Low-grade ($n = 46$)	High-grade ($n = 12$)	
Age (years) (mean ± SD)	55.54 ± 12.40	57.79 ± 14.91	56.83 ± 12.72	68.50 ± 10.88	0.115
Sex					0.648
Female	87 (80.6)	21 (75)	38 (82.6)	6 (50)	
Male	21 (29.4)	7 (25)	8 (17.4)	6 (50)	
Location					0.909
Skull base	28 (26.2)	2 (7.4)	11 (23.9)	3 (25)	
Non-skull base	79 (73.8)	25 (92.6)	35 (76.1)	9 (75)	
Mitosis number† (mean ± SD)	1.20 ± 0.52	7.36 ± 5.41	1.15 ± 0.45	6.63 ± 5.38	0.314
Ki-67 labeling index† (mean ± SD)	1.93 ± 1.29	7.68 ± 5.83	1.59 ± 0.93	6.42 ± 3.79	0.212

Unless otherwise indicated, data are presented as numbers of patients (%)

SD standard deviation

* Calculated from Student's *t* test for continuous variables and chi-square test for categorical variables

† The mitosis number and the Ki-67 labeling index were calculated within patients with available data

The best performance was yielded from a combination of feature selection by RFE and SVM classification algorithm with SMOTE, with an AUC, accuracy, sensitivity, and specificity of 0.86 (95% confidence interval [CI], 0.74–0.98), 89.7%, 75.0%, and 93.5%, respectively. The accuracy was significantly higher than the no-information rate accuracy (79.3%) on validation ($p = 0.03$). Supplementary Fig. 2 shows the receiver operating characteristic and precision-recall curves. Supplementary Fig. 3 shows a heat map according to meningioma grades in the discovery and validation sets, which reveals a strong relationship between texture and morphology features ($p < 0.05$) and meningioma grades.

Relation of texture and morphology parameters with mitosis count and Ki-67 labeling index

Both the mitotic count and the Ki-67 labeling index were significantly correlated with multiple texture and morphology parameters (Supplementary Table 3 and Table 4). Supplementary Fig. 4 shows correlation matrix plots among texture and morphologic features, the mitosis count, and the Ki-67 labeling index ($p < 0.05$).

Texture and morphology analyses according to fibroblastic versus other subtypes

The subtypes of benign meningiomas were divided into 17 fibroblastic and 137 non-fibroblastic (49 meningothelial, 71 transitional, 3 psammomatous, 1 secretory, 7 angiomatous, and 6 microcystic) subtypes. There were significant differences in the various texture parameters between fibroblastic and non-fibroblastic meningioma subtypes (Supplementary Table 5).

Discussion

Preoperative prediction of the meningioma grade is clinically important. Although surgical resection is the primary treatment for meningiomas, observation or gamma knife surgery is considered in patients with asymptomatic small meningiomas without pathological confirmation [35]. Additionally, adjuvant radiotherapy has demonstrated efficacy for high-grade meningiomas [36, 37], whereas the role of adjuvant radiotherapy for low-grade (WHO grade I) meningiomas is unclear [38, 39]. Therefore, we comprehensively analyzed the texture and morphology features of T1C images, ADC, and FA maps, according to the meningioma grades and histologic subtypes. The machine learning classifiers showed fair to excellent performance to predict the meningioma grade in the discovery set (AUC, 0.7–0.1) and fair to good performance in the validation set (AUC 0.74–0.86). In benign meningiomas, there were significant differences in the various texture features between fibroblastic and non-fibroblastic meningioma subtypes.

Spatial and temporal textures are based on the destruction of normal anatomy by tumors, vasogenic edema, tumor cellularity, degenerative changes, or the compression of normal structures, as well as some that the human visual system fails to detect. In fact, the notion that texture analysis can reveal visually imperceptible tumor information extends beyond radiology to histopathology; texture analysis has been reported

Table 2 The performances of machine learning models in differentiating the meningioma grade in the validation set

Model	Feature selection	Subsampling	AUC (95% CI)	Accuracy (%)	Sensitivity (%)	Specificity (%)
RF	None	None	0.74 (0.53–0.94)	84.5	41.7	95.7
		SMOTE	0.84 (0.70–0.98)	87.9	66.7	93.5
		ROSE	0.83 (0.73–0.97)	77.6	75.0	78.3
	RFE	None	0.80 (0.65–0.97)	84.5	41.7	95.7
		SMOTE	0.82 (0.69–0.97)	82.8	58.3	89.1
		ROSE	0.84 (0.70–0.96)	50	100	37.0
SVM	None	None	0.82 (0.69–0.95)	84.5	41.7	95.7
		SMOTE	0.77 (0.59–0.94)	75.9	66.7	78.2
		ROSE	0.83 (0.70–0.96)	82.8	75.0	84.8
	RFE	None	0.85 (0.72–0.98)	82.8	16.7	100
		SMOTE	0.86 (0.74–0.98)	89.7	75.0	93.5
		ROSE	0.85 (0.71–0.98)	84.5	50	93.5

AUC area under the curve, *CI* confidence interval, *RF* random forest, *SVM* support vector machine, *SMOTE* synthetic minority over-sampling technique, *ROSE* random over-sampling examples

to be a potentially useful approach for estimating grades and molecular status in brain tumors [17, 40].

Among conventional MR features, heterogeneous enhancement was reported to be associated with atypical meningiomas [15, 41]. Heterogeneous enhancement is associated with heterogeneous distribution of tumor cells, which reflects intratumoral ischemic necrosis, calcification, hemorrhage, and cystic change. Previous reports have stated that atypical and anaplastic meningiomas have significantly more intratumoral cystic changes, compared with benign meningiomas [42, 43]. These can be quantitatively measured by texture features.

The usefulness of diffusion-weighted imaging in predicting the histological grades of meningiomas is controversial. Several studies have demonstrated significant differences between the grades and ADC values of meningiomas [7–9, 13]. However, other studies have shown that the mean ADC values in meningiomas were not significantly different according to grades [10–12]. In our study, there was no significant difference in the mean ADC or FA values. However, various texture features of ADC and FA maps were significantly different. High-grade meningiomas show a heterogeneous distribution of proliferating cells, resulting in an imbalance of cell density within the tumors [44]. This heterogeneous distribution of cell density was quantified by ADC and FA texture features in our study; high-grade meningiomas showed higher asymmetry, contrast, dissimilarity, and coarseness, as well as less homogeneity along run lengths of ADC and FA values. According to texture features, high-grade meningiomas showed higher histogram entropy, dissimilarity, coarseness, and less homogeneity along the run lengths of T1C, ADC, and FA values. Although we excluded gross cystic or necrotic areas from the radiomics analysis, radiomics features might have reflected microscopic heterogeneity within the tumors. Traditionally, studies including ADC or FA maps have focused on the enhancing solid portion of the tumor, and a recent study using both ADC and T1C radiomics features also performed tumor segmentation only in the enhancing area [45].

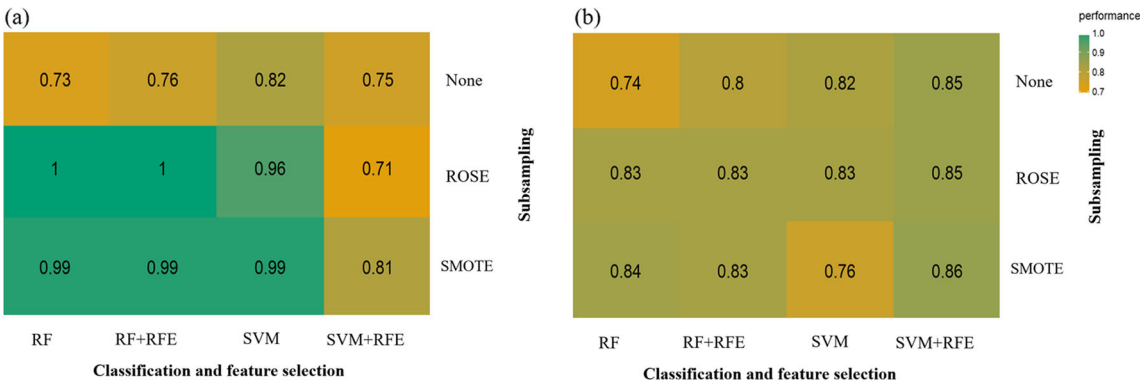

Fig. 3 The heat map of area under the curve (AUC) values from various machine learning classifiers to predict the meningioma grade in the (**a**) discovery and (**b**) validation sets. ROSE, random over-sampling examples; SMOTE, synthetic minority over-sampling technique; RFE, recursive feature elimination; RF, random forest; SVM, support vector machine

A recent study has also reported an association between tumor volume and the histopathological grade of meningioma, which may be due to the relatively high proliferative potential of high-grade tumors [46]. The finding that tumor morphology is an indicator of malignancy has been controversial. Some studies have reported that irregular shape is associated with meningioma aggressiveness [44, 47]. However, another study reported that irregular shape was not significant in a multivariate analysis of high-grade meningioma [15]. A recent study has reported that quantitative shape features were significantly different according to the meningioma grade [40], which is consistent with our results.

A previous study aimed to determine meningioma grades with machine learning based on T1C imaging, but the sample size was smaller with analyses of a single section on the T1C sequence rather than the analysis of the whole tumor, and the data imbalance was not of concern [40]. Due to the relatively low incidence of high-grade meningiomas, data imbalance in meningioma grading is inevitable. Imbalanced datasets can potentially cause a negative effect on fitting of machine learning classification models [30, 48]. In our study, data imbalances were mitigated by using state-of-the-art subsampling techniques that downsample the majority class and synthesize new data points in the minority class, which are recognized as suitable strategies in machine learning [48, 49]. The performance was mostly improved by both ROSE and SMOTE; the best performance was achieved by a combination of feature selection by RFE and SVM classification algorithm with SMOTE, and the accuracy was higher than the no-information rate accuracy. Also, we have assessed the precision-recall curve, which is known to be more informative than the receiver operating characteristic curve for imbalanced datasets [50].

In the present study, various texture and morphology features were correlated with the mitotic count and the Ki-67 labeling index. Previous studies have shown discrepant results regarding the relationship between ADC values (normalized or minimum ADC ratios or mean ADC values) and the Ki-67 labeling index [9, 25, 51]. In our study, there was no significant correlation between the mean ADC and the Ki-67 labeling index (according to Supplementary Table 4). However, various texture and morphology features were significantly correlated with the mitotic count and the Ki-67 labeling index. Mitosis is a complex biological process in which the cell undergoes various morphological transformations [52]; these changes may contribute to the various correlations with the texture and morphology features.

In our study, the texture features were significantly different according to fibroblastic and non-fibroblastic subtypes of meningiomas. Previous studies have shown that DTI-based measurement of FA may aid in predicting subtypes of benign meningiomas [53]. The high degree of anisotropy within fibroblastic meningiomas has been attributed to their high content of intercellular fibers and the fascicular orientation of long spindle-shaped tumor cells [54, 55]. Another study showed that the fibroblastic meningiomas are less vascular than meningothelial meningiomas [56], which may be related to differences in T1C image features. Previous studies to classify meningioma subtypes by texture analyses of histopathologic specimen slides have proven effective [57, 58], and we speculate that tumor imaging may be also effective in classifying meningioma subtypes because of the reflection of underlying histology on MRI [59]. Further studies with larger numbers of meningioma subtypes are required for texture analyses in preoperative differentiation of meningioma subtypes.

Our study had several limitations. First, it was based on a single-center, retrospectively collected dataset. Further studies with external validations are needed for evaluating the generalizability of the machine learning classifiers. Second, $b = 600$ s/mm^2 was used, rather than $b = 1000$ s/mm^2 or higher, to perform DTI. This low b value imaging protocol was initially set up at our hospital due to technical requirements within reasonable acquisition time. Since then, the protocol has not changed in order to obtain subsequent patients with the same protocol. This low b value may have resulted in the overestimation of ADC values because of perfusion effects. However, this would likely have a small influence on the analysis of the differences between meningioma grades, since the entire pixels are affected. Third, only the enhancing portion of the tumor was segmented and evaluated in order to assess both DTI and T1C sequences. Although most studies including ADC or FA maps have focused on the enhancing solid portion of the tumor, other studies including T1C have included the nonenhancing area in the tumor [40, 60]. Further study is indicated to compare the results in different tumor segmentation masks, especially in cases of microcystic meningiomas.

Conclusions

Radiomics feature-based machine learning classifiers of the conventional T1C imaging and DTI may be helpful for the differentiation of low-grade and high-grade meningiomas.

Funding This research received funding from the Basic Science Research Program through the National Research Foundation of Korea (NRF) funded by the Ministry of Science, Information and Communication Technologies, and Future Planning (2017R1D1A1B03030440).

Compliance with ethical standards

Guarantor The scientific guarantor of this publication is Professor Seung-Koo Lee, MD, PhD, from Yonsei University College of Medicine (slee@yuhs.ac).

Conflict of interest The authors of this manuscript declare no relationships with any companies, whose products or services may be related to the subject matter of the article.

Statistics and biometry One of the authors has significant statistical expertise (J.M.O., a biostatistician with 5 years of experience in computational biology).

Informed consent The institutional review board waived the requirement to obtain informed patient consent for this retrospective study.

Ethical approval Institutional Review Board approval was obtained.

Methodology
- Retrospective
- Diagnostic or prognostic study
- Performed at one institution

References

1. Ostrom QT, Gittleman H, Xu J et al (2016) CBTRUS statistical report: primary brain and other central nervous system tumors diagnosed in the United States in 2009–2013. Neuro Oncol 18:v1–v75
2. Willis J, Smith C, Ironside JW, Erridge S, Whittle IR, Everington D (2005) The accuracy of meningioma grading: a 10-year retrospective audit. Neuropathol Appl Neurobiol 31:141–149
3. Kshettry VR, Ostrom QT, Kruchko C, Al-Mefty O, Barnett GH, Barnholtz-Sloan JS (2015) Descriptive epidemiology of World Health Organization grades II and III intracranial meningiomas in the United States. Neuro Oncol 17:1166–1173
4. Modha A, Gutin PH (2005) Diagnosis and treatment of atypical and anaplastic meningiomas: a review. Neurosurgery 57:538–550
5. Goldbrunner R, Minniti G, Preusser M et al (2016) EANO guidelines for the diagnosis and treatment of meningiomas. Lancet Oncol 17:e383–e391
6. Balss J, Meyer J, Mueller W, Korshunov A, Hartmann C, von Deimling A (2008) Analysis of the IDH1 codon 132 mutation in brain tumors. Acta Neuropathol 116:597–602
7. Toh CH, Castillo M, Wong AM et al (2008) Differentiation between classic and atypical meningiomas with use of diffusion tensor imaging. AJNR Am J Neuroradiol 29:1630–1635
8. Watanabe Y, Yamasaki F, Kajiwara Y et al (2013) Preoperative histological grading of meningiomas using apparent diffusion coefficient at 3T MRI. Eur J Radiol 82:658–663
9. Surov A, Gottschling S, Mawrin C et al (2015) Diffusion-weighted imaging in meningioma: prediction of tumor grade and association with histopathological parameters. Transl Oncol 8:517–523
10. Santelli L, Ramondo G, Della Puppa A et al (2010) Diffusion-weighted imaging does not predict histological grading in meningiomas. Acta Neurochir (Wien) 152:1315–1319
11. Jolapara M, Kesavadas C, Radhakrishnan VV et al (2010) Role of diffusion tensor imaging in differentiating subtypes of meningiomas. J Neuroradiol 37:277–283
12. Sanverdi SE, Ozgen B, Oguz KK et al (2012) Is diffusion-weighted imaging useful in grading and differentiating histopathological subtypes of meningiomas? Eur J Radiol 81:2389–2395
13. Nagar VA, Ye JR, Ng WH et al (2008) Diffusion-weighted MR imaging: diagnosing atypical or malignant meningiomas and detecting tumor dedifferentiation. AJNR Am J Neuroradiol 29:1147–1152
14. Hashiba T, Hashimoto N, Maruno M et al (2006) Scoring radiologic characteristics to predict proliferative potential in meningiomas. Brain Tumor Pathol 23:49–54
15. Kawahara Y, Nakada M, Hayashi Y et al (2012) Prediction of high-grade meningioma by preoperative MRI assessment. J Neurooncol 108:147–152
16. Joo B, Han K, Choi YS et al (2018) Amide proton transfer imaging for differentiation of benign and atypical meningiomas. Eur Radiol 28:331–339
17. Park YW, Han K, Ahn SS et al (2018) Whole-tumor histogram and texture analyses of DTI for evaluation of IDH1-mutation and 1p/19q-codeletion status in World Health Organization grade II gliomas. AJNR Am J Neuroradiol 39:693–698
18. Kickingereder P, Bonekamp D, Nowosielski M et al (2016) Radiogenomics of glioblastoma: machine learning–based classification of molecular characteristics by using multiparametric and multiregional MR imaging features. Radiology 281:907–918
19. Kickingereder P, Burth S, Wick A et al (2016) Radiomic profiling of glioblastoma: identifying an imaging predictor of patient survival with improved performance over established clinical and radiologic risk models. Radiology 280:880–889
20. Kashimura H, Inoue T, Ogasawara K et al (2007) Prediction of meningioma consistency using fractional anisotropy value measured by magnetic resonance imaging. J Neurosurg 107:784–787
21. Louis DN, Perry A, Reifenberger G et al (2016) The 2016 World Health Organization classification of tumors of the central nervous system: a summary. Acta Neuropathol 131:803–820
22. Tustison NJ, Avants BB, Cook PA et al (2010) N4ITK: improved N3 bias correction. IEEE Trans Med Imaging 29:1310–1320
23. Shinohara RT, Sweeney EM, Goldsmith J et al (2014) Statistical normalization techniques for magnetic resonance imaging. Neuroimage Clin 6:9–19
24. Cha J, Kim S, Kim HJ et al (2014) Differentiation of tumor progression from pseudoprogression in patients with posttreatment glioblastoma using multiparametric histogram analysis. AJNR Am J Neuroradiol 35:1309–1317
25. Tang Y, Dundamadappa SK, Thangasamy S et al (2014) Correlation of apparent diffusion coefficient with Ki-67 proliferation index in grading meningioma. AJR Am J Roentgenol 202:1303–1308
26. Maes F, Collignon A, Vandermeulen D, Marchal G, Suetens P (1997) Multimodality image registration by maximization of mutual information. IEEE Trans Med Imaging 16:187–198
27. Haralick RM, Shanmugam K, Dinstein I (1973) Textural features for image classification. IEEE Trans Syst Man Cybern:610–621
28. Galloway MM (1975) Texture analysis using gray level run lengths. Comput Gr Image Process 4:172–179
29. Chawla NV, Bowyer KW, Hall LO, Kegelmeyer WP (2002) SMOTE: synthetic minority over-sampling technique. J Artif Intell Res 16:321–357
30. Provost F (2000) Machine learning from imbalanced data sets 101 proceedings of the AAAI'2000 workshop on imbalanced data sets, pp 1–3
31. Kuhn M (2008) Building predictive models in R using the caret package Caret package. J Stat Softw 28:1–26
32. Lunardon N, Menardi G, Torelli N (2014) ROSE: a package for binary imbalanced learning. R Journal 6(1)
33. Torgo L (2013) Package 'DMwR'. Comprehensive R Archive Network
34. van Griethuysen JJM, Fedorov A, Parmar C et al (2017) Computational radiomics system to decode the radiographic phenotype. Cancer Res 77:e104–e107
35. Kollová A, Liscák R, Novotný J Jr, Vladyka V, Simonová G, Janousková L (2007) Gamma Knife surgery for benign meningioma. J Neurosurg 107:325–336
36. Kaur G, Sayegh ET, Larson A et al (2014) Adjuvant radiotherapy for atypical and malignant meningiomas: a systematic review. Neuro Oncol 16:628–636
37. Dziuk TW, Woo S, Butler EB et al (1998) Malignant meningioma: an indication for initial aggressive surgery and adjuvant radiotherapy. J Neurooncol 37:177–188

38. Stafford SL, Pollock BE, Foote RL et al (2001) Meningioma radiosurgery: tumor control, outcomes, and complications among 190 consecutive patients. Neurosurgery 49:1029–1038
39. Maclean J, Fersht N, Short S (2014) Controversies in radiotherapy for meningioma. Clin Oncol (R Coll Radiol) 26:51–64
40. Yan PF, Yan L, Hu TT et al (2017) The potential value of preoperative MRI texture and shape analysis in grading meningiomas: a preliminary investigation. Transl Oncol 10:570–577
41. Lin BJ, Chou KN, Kao HW et al (2014) Correlation between magnetic resonance imaging grading and pathological grading in meningioma. J Neurosurg 121:1201–1208
42. Chen TY, Lai PH, Ho JT et al (2004) Magnetic resonance imaging and diffusion-weighted images of cystic meningioma: correlating with histopathology. Clin Imaging 28:10–19
43. Hsu CC, Pai CY, Kao HW, Hsueh CJ, Hsu WL, Lo CP (2010) Do aggressive imaging features correlate with advanced histopathological grade in meningiomas? J Clin Neurosci 17:584–587
44. Nakasu S, Nakasu Y, Nakajima M, Matsuda M, Handa J (1999) Preoperative identification of meningiomas that are highly likely to recur. J Neurosurg 90:455–462
45. Kang D, Park JE, Kim YH et al (2018) Diffusion radiomics as a diagnostic model for atypical manifestation of primary central nervous system lymphoma: development and multicenter external validation. Neuro Oncol 20:1251–1261
46. Hwang WL, Marciscano AE, Niemierko A et al (2015) Imaging and extent of surgical resection predict risk of meningioma recurrence better than WHO histopathological grade. Neuro Oncol 18: 863–872
47. New PF, Hesselink JR, O'Carroll CP, Kleinman GM (1982) Malignant meningiomas: CT and histologic criteria, including a new CT sign. AJNR Am J Neuroradiol 3:267–276
48. He H, Garcia EA (2009) Learning from imbalanced data. IEEE Trans Knowl Data Eng 21:1263–1284
49. Menardi G, Torelli N (2014) Training and assessing classification rules with imbalanced data. Data Min Knowl Disc 28:92–122
50. Saito T, Rehmsmeier M (2015) The precision-recall plot is more informative than the ROC plot when evaluating binary classifiers on imbalanced datasets. PLoS One 10:e0118432
51. Ginat DT, Mangla R, Yeaney G, Wang HZ (2010) Correlation of diffusion and perfusion MRI with Ki-67 in high-grade meningiomas. AJR Am J Roentgenol 195:1391–1395
52. Jothi JAA, Rajam VMA (2017) A survey on automated cancer diagnosis from histopathology images. Artif Intell Rev 48:31–81
53. Tropine A, Dellani PD, Glaser M et al (2007) Differentiation of fibroblastic meningiomas from other benign subtypes using diffusion tensor imaging. J Magn Reson Imaging 25:703–708
54. Kleihues P, Cavenee WK (2000) Pathology and genetics of tumours of the nervous system, vol 1. International Agency for Research on Cancer, Lyon
55. Wang S, Kim S, Zhang Y et al (2012) Determination of grade and subtype of meningiomas by using histogram analysis of diffusion-tensor imaging metrics. Radiology 262:584–592
56. Maeda M, Itoh S, Kimura H et al (1994) Vascularity of meningiomas and neuromas: assessment with dynamic susceptibility-contrast MR imaging. AJR Am J Roentgenol 163:181–186
57. Fatima K, Arooj A, Majeed H (2014) A new texture and shape based technique for improving meningioma classification. Microsc Res Tech 77:862–873
58. Al-Kadi OS (2010) Texture measures combination for improved meningioma classification of histopathological images. Pattern Recognit 43:2043–2053
59. Gatenby RA, Grove O, Gillies RJ (2013) Quantitative imaging in cancer evolution and ecology. Radiology 269:8–14
60. Zhang Z, Yang J, Ho A et al (2018) A predictive model for distinguishing radiation necrosis from tumour progression after gamma knife radiosurgery based on radiomic features from MR images. Eur Radiol 28:2255–2263